All electrical detection of thermal Hall angle by on-slab thermocouples

Fuyuki Ando,[1,a)] Yuya Sakuraba,[1,a)] Weinan Zhou,[1] Takamasa Hirai,[1] and Ken-ichi Uchida[1,2]

[1]*National Institute for Materials Science, Tsukuba 305-0047, Japan*

[2]*Department of Advanced Materials Science, Graduate School of Frontier Sciences, The University of Tokyo, Kashiwa 277-8561, Japan*

[a)] Authors to whom correspondence should be addressed. ANDO.Fuyuki@nims.go.jp and SAKURABA.Yuya@nims.go.jp

ABSTRACT

We propose a simple and reliable measurement method for the thermal Hall effect by the use of thermocouples fabricated directly on a target material. The thermal Hall angle has been typically characterized by measuring diagonal and off-diagonal terms of thermal conductivity tensor with manually attached bulk thermometers such as thermocouples and resistance temperature sensors. However, the presence of contact thermal resistance between the material and thermometers and the ambiguity of actual temperature information under a magnetic field hinder the quantitative evaluation of the thermal Hall angle. In this work, to characterize the temperature gradient with low contact thermal resistance, we deposit a thermoelectric NiCu thin film directly on the target materials, pattern it into a crossbar shape, and attach two Au wires at the hot and cold junctions to form a closed electrical circuit, i.e., an on-slab thermocouple. Owing to the ideal fourfold symmetry of the structure, we can determine the thermal Hall angle simply from the ratio of the measured thermoelectric voltages in the longitudinal (input) and transverse (output) directions for the on-slab thermocouples under the out-of-plane magnetic field. The measurements for Co_2MnGa Heusler alloy and Ni slabs by the proposed method find that the thermal Hall effect was clearly detected in a wide temperature range from 60 K to 330 K, which is quantitatively consistent with the literature. This approach offers a simple and reliable route to investigate the thermal Hall effect and reveal the wide variety of carrier transport and thermal conversion phenomena.

MANUSCRIPT

Thermal Hall effect (THE), i.e., Righi-Leduc effect is the thermal analog of the electrical Hall effect[1–20]. THE generates a heat current density $\mathbf{j}_{q,THE}$ orthogonal to an input heat current density $\mathbf{j}_{q,in}$ and magnetic field $\mathbf{H}$ with the magnitude H (ordinary THE) or magnetization $\mathbf{M}$ with the magnitude M (anomalous THE) as,

$$\mathbf{j}_{q,THE} = \frac{\kappa_{xy}}{\kappa_{yy}}\mathbf{j}_{q,in} \times \frac{\mathbf{H}}{|H|}\left(\text{or } \frac{\mathbf{M}}{|M|}\right) \quad (1)$$

$$= \tan\theta_{\mathrm{THE}}\,\mathbf{j}_{\mathrm{q,in}} \times \frac{\mathbf{H}}{|H|}\left(\text{or } \frac{\mathbf{M}}{|M|}\right)$$

where κ_{yy} and κ_{xy} are the diagonal and off-diagonal terms of thermal conductivity tensor, respectively, and $\tan\theta_{\mathrm{THE}} = \kappa_{xy}/\kappa_{yy}$ is the thermal Hall angle. Various carriers such as electron, phonon[3,5], and magnon[4,8,10,16], can induce THE reflecting the scattering mechanism[2,7], Berry curvature[5,6,9], and topologically protected edge currents[15,16] in condensed matters including superconductors and insulators. Especially for Kitaev quantum spin liquids, the half-quantized κ_{xy} value is crucial evidence for the existence of the chiral Majorana edge mode[11,14,20]. Meanwhile, the presence of κ_{xy} has an influence on the thermoelectric and thermo-spin conversion phenomena[21–26]. For example, the appearance of a transverse temperature gradient by THE induces the parasitic Seebeck (Nernst) thermopower on the intrinsic transverse (longitudinal) thermopower, resulting in the modulation of thermoelectric performances from those purely by the transverse (longitudinal) thermoelectric effect[25]. Thus, the quantitative evaluation of $\tan\theta_{\mathrm{THE}}$ reveals the wide variety of carrier transport phenomena and develops materials with thermal conversion functionalities.

However, the methodology to determine $\tan\theta_{\mathrm{THE}}$ still has room for improvement with respect to its complexity and reproducibility. The typical $\tan\theta_{\mathrm{THE}}$ analysis relies on the simultaneous measurements of temperature gradients for longitudinal and transverse directions, $\nabla_x T$ and $\nabla_y T$, respectively, under the assumption of a thermally adiabatic condition in the transverse direction ($\mathbf{j}_{\mathrm{q},y} = \kappa_{yx}\nabla_x T + \kappa_{yy}\nabla_y T = 0$), where one can estimate $\tan\theta_{\mathrm{THE}} = \kappa_{xy}/\kappa_{yy} = -\kappa_{yx}/\kappa_{yy}$ as

$$\tan\theta_{\mathrm{THE}} = \nabla_y T/\nabla_x T. \tag{2}$$

A precise temperature measurement to determine $\nabla_x T$ and $\nabla_y T$ is required because the $\tan\theta_{\mathrm{THE}}$ value is usually less than 1%[27]. However, the contact thermal resistances between target materials and thermometers and the deviation from the thermally adiabatic condition are the major sources of errors in this process. Furthermore, the magneto-thermoelectric or magneto-resistance (-capacitance) effect[18] on thermometers need to be taken into account for the accurate estimation of $\tan\theta_{\mathrm{THE}}$, which makes the analysis procedure complicated. To solve these problems, K. Tomioka, K. Uchida, R. Iguchi *et al*. and T. Imamura, T. Hirai, K. Oyanagi *et al*. developed noncontact $\tan\theta_{\mathrm{THE}}$ measurement and analysis methods using periodic-laser-heating-based and magnetic-field-modulation-based lock-in thermography technique under the nearly adiabatic condition[17,19]. Their work offers a higher reliability of $\tan\theta_{\mathrm{THE}}$ than ever before but is hardly applied below room temperature due to a drastic decrease in infrared radiation intensity. Meanwhile, J. Xu, J. He, J.S. Zhou *et al*. developed the electrical detection of THE by the Seebeck voltage contrast using two kinds of wires with different Seebeck coefficients S (Cu and CuNi)[28]. Their study provides an inspiration for the reproducible and versatile method for THE but did not focus on the quantitative evaluation of

$\tan\theta_{\mathrm{THE}}$ by eliminating the parasitic thermoelectric voltage, e.g., the Nernst and spin Seebeck effects derived from the target material. From these backgrounds, a thermal Hall measurement method which one can easily use with high reliability and reproducibility needs to be established.

Here, we propose a simple method to measure $\tan\theta_{\mathrm{THE}}$ based on the on-slab thermocouples. Figure 1(a) shows schematic and photographs of the detailed measurement configuration. A target slab sample with a square-shape is bridged between the heat source and heat sink, where the thermally adiabatic condition is realized by connecting the corners of the slab to the heat source/sink and applying $\mathbf{j}_{\mathrm{q,in}}$ in the diagonal direction. A thermoelectric thin film is directly deposited on the slab to minimize the contact thermal resistance with high reproducibility and patterned into a crossbar shape with a typical microfabrication technique. Metallic wires are attached at the ends of the thermoelectric thin film which serves as the hot and cold junctions of the on-slab thermocouple. Owing to the ideal fourfold symmetry of the crossbar structure with the length $l_x(=l_y)$, $\tan\theta_{\mathrm{THE}}$ can be estimated just from the ratio of the simultaneously measured longitudinal and transverse thermoelectric voltages, V_x and V_y, as below,

$$\begin{aligned} V_y/V_x &= \Delta S\cdot\nabla_y T\cdot l_y/\Delta S\cdot\nabla_x T\cdot l_x \\ &= \tan\theta_{\mathrm{THE}}. \end{aligned} \tag{3}$$

Here, ΔS is the difference in S between the thermoelectric thin film and metallic wire, for which the magnetic field dependence is generally non-zero but cancels out for the estimation of $\tan\theta_{\mathrm{THE}}$. Thus, our method does not need to account the magneto-thermoelectric contribution or convert them into the temperature information. This simple and reliable approach will be a guide in various research fields to easily access THE and reveal the unconventional carrier transport and conversion phenomena.

The fabrication process of the on-slab thermocouple system in this study is as follows. We used polycrystalline CMG and commercially available Ni slabs with a size of 7.0 × 7.0 × 0.8 mm^3 and 7.0 × 7.0 × 0.5 mm^3, respectively. The synthesis process and reference $\tan\theta_{\mathrm{THE}}$ value for CMG slabs were reported in the previous studies[12,17,29,30]. The surface of the CMG and Ni slabs was mechanically polished using sandpapers with the minimum grit of 2000 and abrasive slurry with the alumina particle size of 3, 1, and 0.3 μm for the following deposition of uniform thin films. Figures 1(b) and 1(c) show the ferromagnetic properties of pieces of CMG and Ni measured by a magnetic property measurement system (MPMS; Quantum Design). As shown in Fig. 1(b), M for both samples saturate less than 1 T at 300 K. Then, we define the saturation magnetization M_{sat} by the average M value in the range of 1–2 T of the M-H curve and show the temperature dependence of M_{sat}, where the M_{sat} value is almost constant below 330 K. We used a NiCu film with a composition ratio of Ni:Cu = 45:55 as the on-slab thermocouple material, whose S was measured to be -30.4 μV/K at room temperature by a Seebeck Coefficient / Electric Resistance

Measurement System (ZEM3 M8, ADVANCE RIKO, Inc.). To prevent V_x and V_y from the contamination by the Nernst effect or electrical shunting in the metallic slabs, we first covered a central area of the top surface with a 2-μm-thick insulating epoxy photoresist (SU-8 2002, Kayaku Advanced Materials, Inc.[31]) by a spin coater and cured it at 180°C. The thermal resistance of 2-μm-thick SU-8 layer is roughly estimated to be ~0.3 K/W from the thermal conductivity of 0.3 W/mK[31,32] and the dimension of 5 mm × 5 mm × 2 μm, which is several orders of magnitude smaller than those of commonly used metal wires connecting target materials and bulk thermometers (> 100 K/W)[27]. A crossbar shape with a width of 0.1 mm and a length of 3.8 mm was patterned with a positive resist on the insulating SU-8 layer using the photolithography technique. A 100-nm-thick NiCu thin film was deposited by co-sputtering Ni and Cu at room temperature using dc magnetron sputtering. Finally, a crossbar pattern of NiCu was obtained via a lift-off process. At the ends of the NiCu crossbar, Ta(10 nm)/Au(100 nm) electrodes with a size of 200 × 200 μm^2 were deposited to strictly define the distance between the hot and cold junctions being 3.4 mm as shown in Fig. 1(a). After fixing Au blocks with a size of 200 × 200 × 25 μm^3 on the Au electrodes by silver epoxy, we attached Au wires with S of 1.96 μV/K at room temperature[33] on the Au blocks by a wire bonding method. Because the Ta/Au electrodes and Au blocks are sufficiently thin, the temperature difference appears mainly in the in-plane direction of the NiCu thin film and in the Au wires connecting the NiCu to the isothermal sample holder electrodes. The electrical insulation between the CMG slab and on-slab thermocouples (> 20 MΩ) was confirmed by a multimeter. Thus, both the electrical insulation and low thermal resistance were achieved by the 2-μm-thick SU-8 layer.

We observed the in-plane temperature distribution on the CMG and Ni samples under the application of $\nabla_x T$ using infrared thermography. The samples with the SU-8/NiCu/Au films was placed on a homemade holder with a multifunction probe for a physical property measurement system (PPMS; Quantum Design), bridged between two Cu blocks in the x-direction with a distance of ~8 mm, one of which acted as a heat source by applying a heater power P_{in} in an embedded chip heater and the other as a heat sink to apply $\nabla_x T$. The top surfaces of the samples were covered with black ink having an emissivity over 0.94 and observed by an infrared camera at room temperature and atmospheric pressure in the absence of a magnetic field. Figure 2(a) shows a thermography image for the CMG sample captured after applying P_{in} of 0.36 W and waiting for 15 min to stabilize $\nabla_x T$. The area without black ink coating apparently shows lower temperature because of the lower infrared radiation intensity. If the SU-8 layer has a large thermal resistance yielding any temperature difference between the CMG top surface and on-slab thermocouples, the top-view temperature distribution shows a discontinuity between the CMG and SU-8 layer top surfaces. However, the temperature distribution covered with the black ink continuously changes at the edges of the insulating SU-8 layer, which validates a negligibly small contact thermal resistance between the CMG sample and on-slab thermocouples. To characterize $\nabla_x T$ and $\nabla_y T$ on the NiCu crossbar, we obtain line profiles for 3.4 × 0.5 mm^2 [red rectangular area in Fig. 2(a)] and

0.5×3.4 mm^2 [blue rectangular area in Fig. 2(a)], respectively. Figure 2(b) shows the longitudinal temperature distribution in the red and blue rectangular areas under various P_{in} for the CMG sample, where an almost linear slope ensures the homogeneous $\nabla_x T$ in the region of interest. The difference in $\nabla_x T$ between the red and blue rectangular areas are 9.5 for CMG and 13.5% for Ni, which deviations are inevitable in this diagonal configuration due to the nonuniform heat currents. In this work, to take this nonlinearity of $\nabla_x T$ into account, $\tan\theta_{\mathrm{THE}}$ is defined as $1.095 \times V_y/V_x$ for CMG and $1.135 \times V_y/V_x$ for Ni. Meanwhile, Fig. 2(c) shows the transverse temperature distribution in the blue rectangular area under various P for the CMG sample. Under P_{in} of 0.36 W, $\nabla_y T$ is estimated to be 0.004 ± 0.007 K/mm by the slope of linear fit while $\nabla_x T$ being -1.256 ± 0.004 K/mm. Thus, under no magnetic field, the applied temperature gradient is solely along x-direction ($\nabla_y T = 0$).

We measured the magnetic field dependence of V_x and V_y under various P_{in}. In the PPMS chamber with a purged state (vacuum level is about 10 Torr of He gas), V_x and V_y were measured using dc nanovoltmeters (Keithly 2182) after reaching each magnetic field and waiting 20 s to stabilize at the thermal equilibrium state. The PPMS cryostat enables a stable temperature and magnetic field control suitable for the sensitive THE measurement[27]. Figure 3(a) shows the result of V_x for the CMG sample at 300 K. The V_x values are hardly changed by the application of the magnetic field, which is one of the characteristics of the NiCu-based alloy and preferable for the thermal Hall measurement. Figure 3(b) shows the average V_x ($V_{x,\mathrm{ave}}$) values for various P_{in} in Fig. 3(a) as a function of ΔT_x obtained from results in Fig. 2(b). The thermopower of the NiCu/Au-based on-slab thermocouple is characterized to be -29.7 μV/K from the slope of linear fit, which agrees with ΔS between the NiCu thin film and Au wire (= S_{NiCu}-S_{Au} = -32.4 μV/K). Thus, V_x is purely attributed to the thermoelectric voltage of the on-slab thermocouple. Meanwhile, Fig. 3(c) shows the magnetic field dependence of V_y for the CMG sample at 300 K. The V_y values reverse depending on the sign of the applied magnetic field and saturate less than 1 T, which obviously reflects the magnetization process of the CMG sample in Fig. 1(b). Thus, the observed V_y predominantly originates from the anomalous THE in the CMG sample. In this study, the saturated V_y ($V_{y,\mathrm{sat}}$) is defined as the average V_y above 1 T to estimate the anomalous thermal Hall angle $\tan\theta_{\mathrm{ATHE}}$ with the negligible contribution of the ordinary THE. Figure 3(d) shows a plot of $V_{y,\mathrm{sat}}$ as a function of the average V_x ($V_{x,\mathrm{ave}}$) to directly estimate $\tan\theta_{\mathrm{ATHE}}$ from the slope of the linear fit with the standard deviation. As a result, we determine the $\tan\theta_{\mathrm{ATHE}}$ values of the polycrystalline CMG to be 2.45 ± 0.02% at 300 K, which is comparable to the literature values (2.65 and 2.94%)[12,17], ensuring the reliability of the proposed method. The lower $\tan\theta_{\mathrm{ATHE}}$ value than that measured in Ref. 17 is attributed to the lower sintering temperature (850°C) of the CMG polycrystal resulting in the relatively disordered $L2_1$-type structure.

Now we are in a position to characterize the thermal Hall effect in the wide temperature range. Figure 4(a) shows the magnetic field dependence of $\tan\theta_{\mathrm{THE}}$ at 60, 180, and 300 K for the CMG sample. In this temperature range, $\tan\theta_{\mathrm{THE}}$ clearly reflects the magnetization curves of CMG saturating less than 1 T, which confirms the validity to use $V_{y,\mathrm{sat}}$ for the determination of $\tan\theta_{\mathrm{ATHE}}$. Figure 4(b) shows $\tan\theta_{\mathrm{ATHE}}$ at temperatures ranging from 60 K to 330 K for the CMG and Ni samples, where $\tan\theta_{\mathrm{ATHE}}$ of -0.53 ± 0.02% at 300 K for the Ni sample agrees with those in the literature (-0.45 and -0.51%)[17,34] as well as the CMG sample. The $\tan\theta_{\mathrm{ATHE}}$ values for the CMG sample show the increase trend as temperature increases with the small error bars differing from the magnetization behavior in Fig. 1(c). To explain this temperature dependence of the anomalous THE, L. Xu, X. Li, L. Ding *et al*. confirmed that the anomalous transverse version of the Wiedemann-Franz law held in the CMG system[12], which is a linear relationship between the anomalous Hall effect and anomalous THE: κ_{xy}^{A} is estimated as $L_{xy}^{\mathrm{A}}\sigma_{xy}^{A}T$ with L_{xy}^{A} being the anomalous transverse Lorenz number independent of temperature and σ_{xy}^{A} being the anomalous Hall conductivity[35,36]. Because σ_{xy}^{A} and κ_{yy} of the CMG system show the moderate temperature dependence from 60 K to 330 K, $\tan\theta_{\mathrm{ATHE}}$ $(=\kappa_{xy}^{A}/\kappa_{yy})$ monotonically increases with increasing temperature[12].

To confirm the robustness of our method in the wide temperature range, we performed a thermal cycle test using the Ni sample in the order 330, 60, 330, 60, and 330 K. Figure 4(c) shows the magnetic field dependence of $\tan\theta_{\mathrm{THE}}$ measured at 330 K for three times, where the similar thermal Hall signals are obtained even after the Ni sample experienced the temperature sweep from 60 K to 330 K. As a result, the estimated $\tan\theta_{\mathrm{ATHE}}$ values for 60 and 330 K are reproduced under this thermal cycle condition [Fig. 4(d)], which ensures that the on-slab thermocouple system is mechanically stable against the temperature.

Finally, we note the future perspective and limitation of our proposed method. In this study, we chose the polycrystalline CMG slab with the large $\tan\theta_{\mathrm{ATHE}}$ to demonstrate the validity of our method. However, the characterization of $\tan\theta_{\mathrm{THE}}$ lower than 1% for other materials might be problematic especially at cryogenic temperature. In Fig. 4(a), the signal-to-noise ratio of $\tan\theta_{\mathrm{THE}}$ decreases as temperature decreases due to not only the decrease in $\tan\theta_{\mathrm{THE}}$ of the CMG sample but also the decrease in *S* of the NiCu thin film, which is a typical behavior of the Seebeck effect in metals. Thus, to study the cryogenic phenomena such as the phonon Hall and quantum thermal Hall effects, the development of on-slab resistance temperature sensors instead of thermocouples is required. For the requirement of the deposition and microfabrication of uniform thin films, our proposed method is limited to the materials whose surface can be processed into the mirror finish by mechanical or chemical polishing.

In conclusion, we propose a simple and reliable measurement method for $\tan\theta_{\mathrm{THE}}$ based on the on-slab thermocouples. The on-slab thermocouples minimize the contact thermal resistance between target materials and thermocouples and simplify the $\tan\theta_{\mathrm{THE}}$ analysis process just from the ratio of the longitudinal and transverse thermoelectric voltages without considering

the magneto-thermoelectric effect or converting them into temperatures and thermal conductivities. As the proof-of-concept demonstration, we prepared a NiCu/Au-based on-slab thermocouples on the CMG sample and performed the $\tan\theta_{\mathrm{THE}}$ measurement in the wide temperature range. The $\tan\theta_{\mathrm{ATHE}}$ values show the increase trend following the anomalous transverse Wiedemann-Franz law of CMG with small error bars and quantitatively agree with the literature values measured around room temperature. This simple and reliable method will be helpful to easily measure $\tan\theta_{\mathrm{THE}}$ and reveal the rich variety of carrier transport and conversion phenomena.

The authors thank K. Suzuki, M. Isomura, N. Kojima, and S. Kuramochi for technical support. This work was supported by ERATO "Magnetic Thermal Management Materials" (Grant No. JPMJER2201) from JST, Japan, and Grant-in-Aid for Scientific Research (KAKENHI; Grant No. 24K17610) from JSPS, Japan.

AUTHOR DECLARATIONS

Conflict of Interest

The authors have no conflicts to disclose.

DATA AVAILABILITY

The data that support the findings of this study are available from the corresponding author upon reasonable request.

REFERENCES

[1] A.W. Smith, and A.W. Smith, Phys. Rev. **5**, 35 (1915).

[2] Y. Zhang, N.P. Ong, Z.A. Xu, K. Krishana, R. Gagnon, and L. Taillefer, Phys. Rev. Lett. **84**(10), 2219 (2000).

[3] C. Strohm, G.L.J.A. Rikken, and P. Wyder, Phys. Rev. Lett. **95**(15), 155901 (2005).

[4] Y. Onose, T. Ideue, H. Katsura, Y. Shiomi, N. Nagaosa, and Y. Tokura, Science **329**(5989), 297–299 (2010).

[5] T. Qin, J. Zhou, and J. Shi, Phys. Rev. B **86**(10), 104305 (2012).

[6] L. Zhang, New J. Phys. **18**(10), 103039 (2016).

[7] K. Sugii, M. Shimozawa, D. Watanabe, Y. Suzuki, M. Halim, M. Kimata, Y. Matsumoto, S. Nakatsuji, and M. Yamashita, Phys. Rev. Lett. **118**(14), 145902 (2017).

[8] S. Murakami, and A. Okamoto, J. Phys. Soc. Jpn. **86**, 011010 (2017).

[9] X. Li, L. Xu, L. Ding, J. Wang, M. Shen, X. Lu, Z. Zhu, and K. Behnia, Phys. Rev. Lett. **119**(5), 056601 (2017).

[10] T. Ideue, T. Kurumaji, S. Ishiwata, and Y. Tokura, Nat. Mater. **16**, 797–802 (2017).

[11] Y. Kasahara, T. Ohnishi, Y. Mizukami, O. Tanaka, S. Ma, K. Sugii, N. Kurita, H. Tanaka, J. Nasu, Y. Motome, T. Shibauchi, and Y. Matsuda, Nature **559**, 227–231 (2018).

[12] L. Xu, X. Li, L. Ding, T. Chen, A. Sakai, B. Fauqué, S. Nakatsuji, Z. Zhu, and K. Behnia, Phys. Rev. B **101**(18), 180404(R) (2020).

[13] K. Uchida, and R. Iguchi, J. Phys. Soc. Jpn. **90**, 122001 (2021).

[14] T. Yokoi, S. Ma, Y. Kasahara, S. Kasahara, T. Shibauchi, N. Kurita, H. Tanaka, J. Nasu, Y. Motome, C. Hickey, S. Trebst, and Y. Matsuda, Science **373**(6554), 568–572 (2021).

[15] R.P. Madhogaria, S. Mozaffari, H. Zhang, W.R. Meier, S.H. Do, R. Xue, T. Matsuoka, and D.G. Mandrus, Phys. Rev. B **108**(12), 125114 (2023).

[16] H.L. Kim, T. Saito, H. Yang, H. Ishizuka, M.J. Coak, J.H. Lee, H. Sim, Y.S. Oh, N. Nagaosa, and J.G. Park, Nat. Commun. **15**, 243 (2024).

[17] T. Imamura, T. Hirai, K. Oyanagi, R. Iguchi, K. Takamori, S. Kobayashi, and K. Uchida, Phys. Rev. Appl. **23**(2), 024018 (2025).

[18] C. Tinsman, G. Li, C. Su, T. Asaba, B. Lawson, F. Yu, and L. Li, Appl. Phys. Lett. **108**, 261905 (2016).

[19] K. Tomioka, K. Uchida, R. Iguchi, and H. Nagano, J. Appl. Phys. **128**, 215103 (2020).

[20] E. Lefrançois, G. Grissonnanche, J. Baglo, P. Lampen-Kelley, J.Q. Yan, C. Balz, D. Mandrus, S.E. Nagler, S. Kim, Y.J. Kim, N. Doiron-Leyraud, and L. Taillefer, Phys. Rev. X **12**(2), 021025 (2022).

[21] H.B. Callen, Phys. Rev. **85**(1), 16–19 (1952).

[22] F. Ando, T. Hirai, A. Alasli, H. Sepehri-Amin, Y. Iwasaki, H. Nagano, and K. Uchida, Energy Environ. Sci. **18**, 4068–4079 (2025).

[23] A. Takahagi, T. Hirai, A. Alasli, S.J. Park, H. Nagano, and K. Uchida, Nat. Phys. **21**, 1283–1289 (2025).

[24] F. Ando, T. Hirai, H. Adachi, and K. Uchida, Phys. Rev. Appl. **23**(6), 064061 (2025).

[25] H. Adachi, F. Ando, T. Hirai, R. Modak, M. Grayson, and K. Uchida, Appl. Phys. Express **18**(9), 090101 (2025).

[26] Y. Lee, F. Ando, T. Hirai, R. Modak, H. Sepehri-Amin, and K. Uchida, Ann. Phys. **537**, e00127 (2025).

[27] H.-L. Kim, M.J. Coak, J.C. Baglo, K. Murphy, R.W. Hill, M. Sutherland, M.C. Hatnean, G. Balakrishnan, and J.-G. Park, Rev. Sci. Instrum. **90**, 103904 (2019).

[28] J. Xu, J. He, J.S. Zhou, D. Qu, S.Y. Huang, and C.L. Chien, Phys. Rev. B **109**(2), L020401 (2024).

[29] T. Hirai, F. Ando, H. Sepehri-Amin, and K. Uchida, Nat. Commun. **15**, 9643 (2024).

[30] K. Oyanagi, H. Sepehri-Amin, K. Takamori, T. Tadano, T. Imamura, R. Nagasawa, K. Mahalingam, T. Hirai, F. Ando, Y. Sakuraba, S. Kobayashi, and K. Uchida, Acta Mater. **296**, 121239 (2025).

[31]"SU-8 2000 Permanent Negative Epoxy Photoresist," Https://Kayakuam.Com/Su-8-2000/.

[32] K.G. Biswas, T.D. Sands, B.A. Cola, and X. Xu, Appl. Phys. Lett. **94**, 223116 (2009).

[33] N. Cusack, and P. Kendall, Proc. Phys. Soc. **72**, 898 (1958).

[34] Y. Onose, Y. Shiomi, and Y. Tokura, Phys. Rev. Lett. **100**, 016601 (2008).

[35] X. Li, L. Xu, L. Ding, J. Wang, M. Shen, X. Lu, Z. Zhu, and K. Behnia, Phys. Rev. Lett. **119**, 056601 (2017).

[36] L. Xu, X. Li, X. Lu, C. Collignon, H. Fu, J. Koo, B. Fauqué, B. Yan, Z. Zhu, and K. Behnia, Sci. Adv. **6**, eaaz3522 (2020).

FIGURES

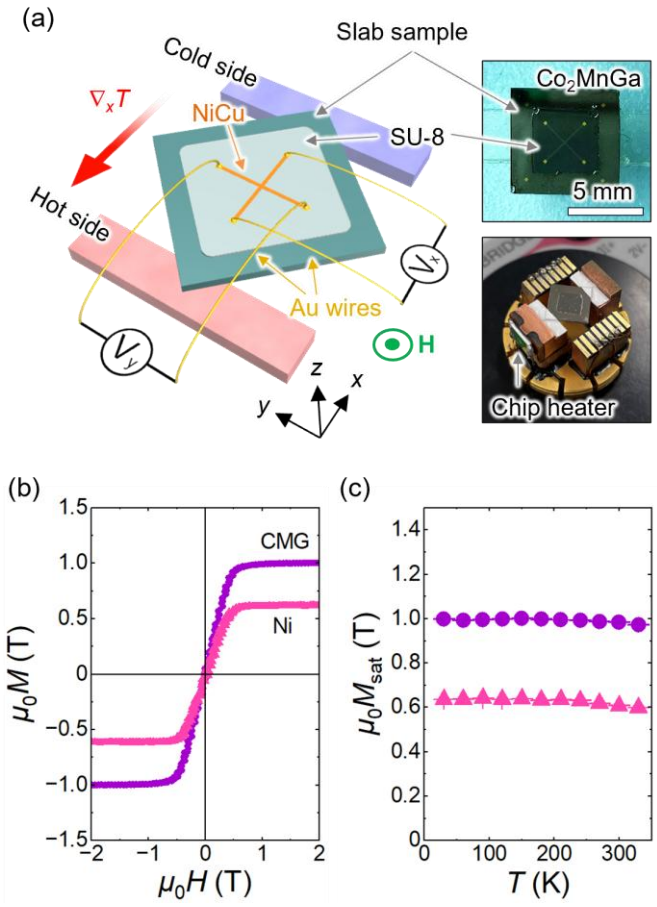

FIG. 1. (a) Schematic and photographs of thermal Hall measurement configuration using the NiCu/Au-based on-slab thermocouples. The photographs show the Co_2MnGa (CMG) Heusler alloy slab sample and the measurement setup on a homemade sample holder. (b) Magnetic field H dependence of the magnetization M and (c) temperature T dependence of the saturation magnetization M_{sat} for CMG and Ni.

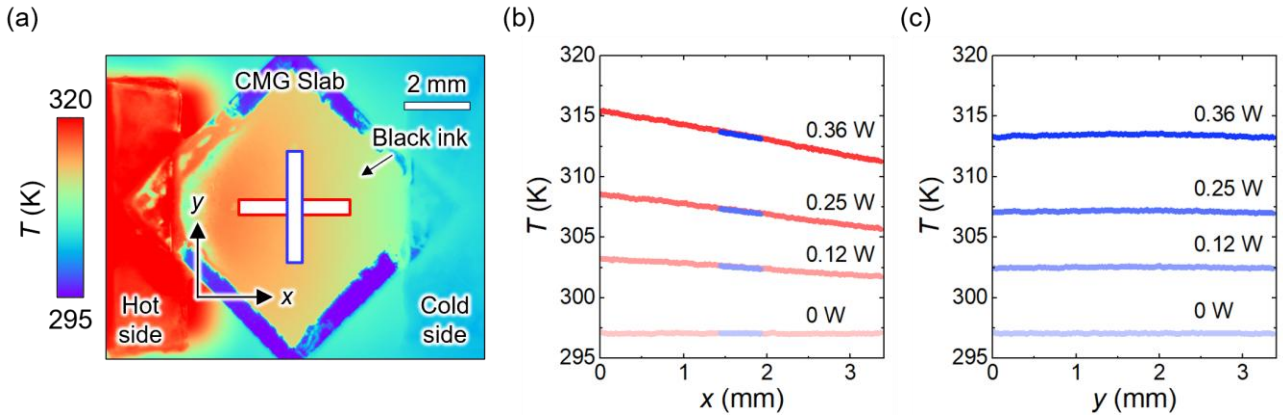

FIG. 2. (a) A thermography image for the CMG sample captured under a heater power P_{in} of 0.36 W at room temperature. (b) Longitudinal T distributions in the red and blue rectangular areas and (c) transverse T distributions in the blue rectangular area in (a) under various P_{in}.

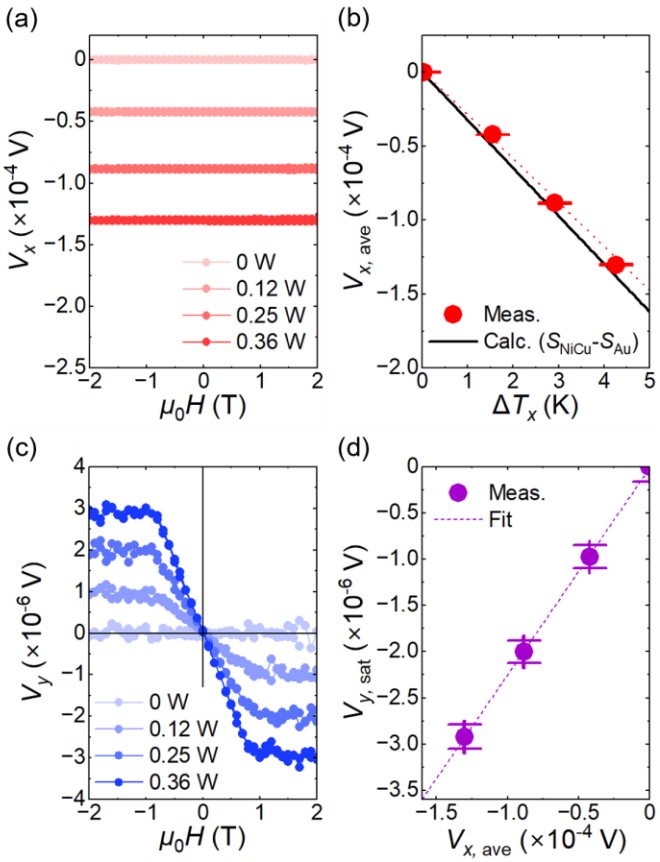

FIG. 3. (a) H dependence of the longitudinal thermoelectric voltage V_x under various P_{in} at 300 K for the CMG sample. (b) The average V_x ($V_{x,\mathrm{ave}}$) as a function of longitudinal temperature difference ΔT_x for various P_{in}. The calculation curve represents the difference in the Seebeck coefficients between the NiCu thin film and Au wire. (c) H dependence of the transverse thermoelectric voltage V_y under various P_{in} at 300 K for the CMG sample. (d) The saturation V_y ($V_{y,\mathrm{sat}}$) as a function of $V_{x,\mathrm{ave}}$ to estimate the anomalous thermal Hall angle $\tan\theta_{\mathrm{ATHE}}$.

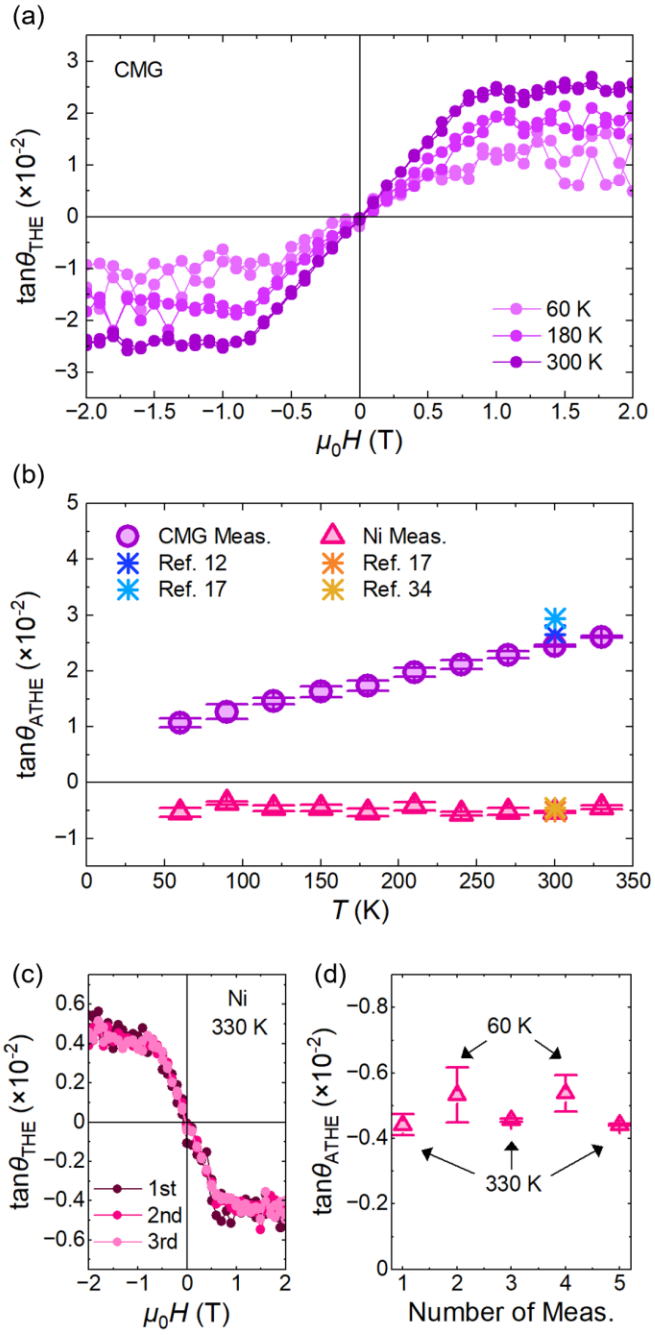

FIG. 4. (a) H dependence of $\tan\theta_{\mathrm{THE}}$ at various T under P_{in} of 0.36 W for the CMG sample. (b) T dependence of $\tan\theta_{\mathrm{ATHE}}$ from 60 K to 330 K for the CMG and Ni samples with the reference values[12,17,34]. (c) H dependence of $\tan\theta_{\mathrm{THE}}$ at 330 K under P_{in} of 0.36 W for the Ni sample before and after the thermal cycle from 60 K to 330 K. (d) Variation of $\tan\theta_{\mathrm{ATHE}}$ at 60 and 330 K during the thermal cycle for the Ni sample.